Control and Cybernetics

vol. **48** (2019) No. 4

ANFIS-based PID continuous sliding mode controller for robot manipulators in joint space*

by

Wael M. Elawady[1], Mohammed F. Asar[2] and Amany M. Sarhan[2]

[1]Department of Computers and Control Engineering,
Tanta University, Egypt, currently, lecturer at the Higher Institute of
Engineering and Technology in Kafr Elsheikh (HIET), Egypt
wmeana2007@yahoo.com
[2] Department of Computers and Control Engineering,
Tanta University, Egypt
asar509@hotmail.com; amany_m_sarhan@yahoo.com

Abstract: This paper presents a feasible design for a control algorithm to synthesize an adaptive neuro-fuzzy inference system-based PID continuous sliding mode control system (ANFIS-PIDCSMC) for adaptive trajectory tracking control of the rigid robot manipulators (RRMs) in the joint space. First, a PID sliding mode control algorithm with sliding surface dynamics-based continuous proportional-integral (PI) control action (PIDSMC-SSDCPI) is presented. The global stability conditions are formulated in terms of Lyapunov full quadratic form such that the robot system output can track the desired reference output. Second, to increase the control system robustness, the PI control action in the PIDSMC-SSDCPI controller is supplanted by an ANFIS control signal to provide a control approach that can be termed adaptive neuro-fuzzy inference system-based PID continuous sliding mode control system (ANFIS-PIDCSMC). For the proposed control algorithm, numerical simulations using the dynamic model of RRM with uncertainties and external disturbances show high quality and effectiveness of the adopted control approach in high-speed trajectory tracking control problems. The simulation results that are compared with the results, obtained for the traditional controllers (standalone PID and traditional sliding mode controller (TSMC)), illustrate the fact that the tracking control behavior of the robot system achieves acceptable tracking performance.

Keywords: PID, continuous sliding mode control, ANFIS, uncertainties, robot

*Submitted: July 2019; Accepted: November 2019.

1. Introduction

Robot manipulator control systems are becoming increasingly important in research and industry (see, e.g., Siciliano et al., 2009; Siciliano and Khatib, 2008). The main challenge in the motion control problem of rigid manipulators is the complexity of their dynamics and the presence of uncertainties (Siciliano et al., 2009; Siciliano and Khatib, 2008; Capisani, Ferrara and Magnani, 2007; Alavandar and Nigam, 2009a,b). A variety of approaches have been proposed in the past decade to deal with the motion control of robot manipulators with uncertainty (see Ho, Wong and Rad, 2007; Cheng, Guang Hou and Tan, 2009; Capisani, Ferrara and Magnani, 2007; Barambones and Etxebarria, 2000; Ortega and Spong, 1989).

Sliding mode control (SMC) (see, e.g., Bharath et al., 2017; Komsta, Oijen and Antoszkiewicz, 2013; Wang et al., 2014; Mahmoodabadi, Taherkhorsandi and Bagheri, 2014; Prasad, Pulwar and Lishor, 2017) has been considered a hot research field for its robustness regarding modeling and control in the presence of uncertainties and external disturbances (Hui et al., 2014; Hu et al., 2012; Li, Li and Li, 2012; Mahmoodabadi, Taherkhorsandi and Bagheri, 2014; Ouyang, Acob and Pano, 2014; Sun et al., 2011; Utkin, Guldner and Shi, 2000; Xiang and Chen, 2011; Chang, 2000). However, SMC suffers from definite drawbacks (see Ouyang, Acob and Pano, 2014). First, it is generally difficult to obtain perfect dynamical models for highly coupled nonlinear systems. Secondly, the chattering phenomenon will often excite high frequency dynamics of the system (Zeinali and Notash, 2010; Chang, 2000). Moreover, a priori knowledge of the upper bounds of the norm of the perturbation vector is required to obtain robustness and convergence (Zeinali and Notash, 2010).

The design of robust adaptive controller without knowledge of the upper bound of uncertainties was presented in Su and Leung (1993), Elmali and Olgac (1992), Yu and Lloyd (1997), Gong and Yao (1999), and Zeinali and Notash (2010). In Choi and Cheol Lee (2009), a proportional-integral-derivative, PID-based sliding mode controller using an observer was also proposed to solve the chattering problem of sliding mode control. In Zeinali and Notash (2010), the authors exploited the adaptive control technology and the sliding mode control theory to adopt controller, in which the discontinuous control effect of the SMC is replaced by a smooth continuous control term that is based on the dynamics of the sliding surface. The control algorithm, adopted in Zeinali and Notash (2010), used a model-based control term and an uncertainty observer to estimate the perturbation from the sliding surface dynamics. The authors of Jafarov, Parlakçi and Istefanopoulos (2005) proposed the PID sliding mode controller with PID sliding surface, in which the conventional equivalent control term is not used, because the controller needs to use the exact full robot dynamics knowledge, which involves unavailable parameter uncertainties..

However, the control law in Jafarov, Parlakçi and Istefanopoulos (2005) involves the discontinuous signum function, which causes serious chattering phenomenon.

The adaptive neuro-fuzzy inference system (ANFIS) (see Melin and Castillo, 2005; Bhattacharyya et al., 2015; Kar, Das and Ghosh, 2014), proposed by Jang (Jang, 1993) as a hybrid intelligent system, is one of the most widely used fuzzy inference systems. It is constructed from a framework of adaptive neural networks embedded with the fuzzy inference systems (Kar, Das and Ghosh, 2014). The authors of Alavandar and Nigam (2009c) presented a new hybrid adaptive neuro-fuzzy control algorithm (ANFIS) for manipulator control with uncertainties. The hybrid controller consists of adaptive neuro-fuzzy controller and conventional controller such that the outputs of these controllers are augmented with ANFIS control signal to generate the final actuation signal.

Motivated by the investigations mentioned above, this paper is concerned with the problem of designing robust adaptive control algorithms meant to tackle the stabilizing and tracking problems of RRMs with structured and unstructured uncertainties in dynamics, and to achieve effective elimination of the inherent drawbacks of the previous work (see Jafarov, Parlakçi and Istefanopoulos, 2005; Zeinali and Notash, 2010, and Alavandar and Nigam, 2009c) without involving sophisticated mathematics, as well as to increase system robustness against parameter uncertainty, load disturbance and nonlinearities.

As an extended control methodology relative to the developments presented in Jafarov, Parlakçi and Istefanopoulos (2005), Zeinali and Notash (2010) and Alavandar and Nigam (2009c), first, a PID sliding mode control algorithm with sliding surface dynamics-based continuous proportional-integral (PI) control action (PIDSMC-SSDCPI) is presented. In this control methodology, the equivalent control term in TSMC is replaced by PID controller with feedback relay control action, and the discontinuous control signal of TSMC is replaced by a sliding surface dynamics-based continuous proportional-integral (SSDCPI) control action. The overall closed-loop control system guarantees the global asymptotic stability and the global stability conditions are formulated in terms of Lyapunov full quadratic form, such that the robot system output can track the desired reference output asymptotically under the conditions of parameter variations, modeling uncertainties, external disturbances and nonlinear friction. Second, to increase the control system robustness and suppress the effects of un-modeled dynamics and external disturbances on the trajectory tracking error, the PI control action in the PIDSMC-SSDCPI controller is supplanted by an ANFIS control signal (Alavandar and Nigam, 2009c) to provide a control approach that can be termed adaptive neuro-fuzzy inference system-based PID continuous sliding mode control system (ANFIS-PIDCSMC).

The simulations have been carried out to evaluate the effectiveness of the proposed control algorithm for robot manipulator arm motion control. The proposed methodology is compared with conventional controllers (TSMC and standalone PID). The simulation results demonstrated that the behavior of the proposed algorithm is superior to the traditional ones. The remainder of this paper is organized as follows: Section 2 presents the characteristics of the proposed PID continuous sliding mode control algorithm with continuous control action, Section 3 describes the stability analysis of the proposed PIDSMC-SSDCPI, Section 4 presents the ANFIS-based PID continuous sliding mode controller, Section 5 provides the simulation results and Section 6 summarizes the conclusions of the work.

2. PID continuous sliding mode control algorithm with continuous control action

The Euler-Lagrange dynamic equations for an n-link robot are given by (see Abdallah et al., 1991; Siciliano et al., 2009, Cheng, Guang Hou and Tan, 2009):

$$B(q)q'' + C(q,q')q' \; + \; F_d\, q' + F_s(q') + \tau_d(t) + g(q) \; = \; \tau \tag{1}$$

where q, q', $q'' \in R^n$ are the joint position, velocity, and acceleration vectors, respectively; $B(q)$ denotes the $n \times n$ bounded positive definite inertia matrix; $C(q,q')$ expresses the $n \times n$ Coriolis, centripetal matrix; $g(q)$ is the gravity vector; $F_d \in R^{n\times n}$ and $F_s(q') \in R^n$ represent the dynamic friction coefficient matrix and static friction vector, respectively; $\tau_d(t)$ is the vector of disturbances and un-modeled dynamics; $u(t) = \tau$ is the control vector representing the torque exerted on joints. In general, the robot parameters of mass, inertia, Coriolis and centrifugal force effect, friction, and gravity effects involve a nominal part and some variation, therefore, in the presence of the model uncertainties and external disturbances, Eq. (1) can be written down as

$$(B(q)+\Delta B)\, q''+(C(q,q')+\Delta C)q' + F_d\, q'+F_s(q')+\tau_d(t)+(g(q)+\Delta g) \; = \; \tau \tag{2}$$

where $\Delta B(q)$, $\Delta C(q,q')$ and $\Delta g(q)$ are the unknown parts of the robot inertia, Coriolis and centrifugal forces effect, and gravity torques, respectively.

By rearranging the terms in Eq. (2), we obtain:

$$B(q)q''+C(q,q')q'+g(q)+\Delta B\, q''+\Delta C q''+\Delta g+ F_d\, q'+F_s(q')+\tau_d(t) \; = \; u(t). \tag{3}$$

It is assumed that all uncertain elements can be lumped as follows:

$$d(t) = -\left\{\Delta B(q)\, q'' + \Delta q' + \Delta g \; + \; F_d\, q' + F_s(q') + \tau_d(t)\right\}. \tag{4}$$

The dynamics model is written down then as:

$$q'' = -B^{-1}\left\{C(q,q')q' + g(q) - d(t)\right\} \; + B^{-1}u(t) \tag{5}$$

where $d(t)$ represent the uncertainty vector of the direct dynamics that consists of the vectors of all uncertainties including external disturbances.

The PID sliding surface $s(t)$ in the space of tracking error can be defined as in Jafarov, Parlakçi and Istefanopoulos (2005) and Zeinali and Notash (2010), namely:

$$s(t) = K_d e'(t) + K_p e(t) + K_i \int e(t)dt \tag{6}$$

where $s(t)$ is an $n \times 1$ vector representing the sliding surface; K_p is an $n \times n$ diagonal positive definite proportional gain matrix, K_i is an $n \times n$ diagonal positive definite integral gain matrix, K_d is an $n \times n$ diagonal positive definite derivative gain matrix, being the parameters to be selected and $e(t) = q(t) - q_d(t)$ is the tracking position error vector, in which $q_d(t)$ is the desired trajectory vector.

For the tracking control problem of RRM, a control input $u(t)$ that represents the vector of the torques applied to the joints is designed in such a manner that the error state trajectory is kept on the sliding surface $s(t) = 0$ for all the time $t > 0$. To achieve this objective, the proposed PID sliding mode control algorithm with sliding surface dynamics based continuous proportional-integral (PI) control action (PIDSMC-SSDCPI) is chosen as:

$$u(t, s) = u_{PID}(t) + u_{SSDCPI}(t, s), \tag{7}$$

where $u_{PID}(t)$ and $u_{SSDCPI}(t, s)$ are the PID control and the sliding surface dynamics based continuous proportional-integral (PI) control actions, respectively. The PID control term, $u_{PID}(t)$, has the advantages of a simple structure, clear functionality and easy implementation, and it replaces the equivalent control term of the traditional sliding mode control (TSMC), which is not utilized because it requires perfect knowledge of the mathematical model of robot dynamics. The continuous proportional-integral (PI) control action based on sliding surface dynamics, $u_{SSDCPI}(t, s)$, replaces the discontinuous control term of TSMC, which eliminates the chattering problem of TSMC, while preserving fast convergence and system robustness against parameter uncertainty, load disturbance, and nonlinearities.

3. Stability analysis of the proposed PIDSMC-SSDCPI

Lyapunov stability approach is employed to investigate the stability property of the proposed controller. The Lyapunov function candidate is defined as in Jafarov, Parlakçi and Istefanopoulos (2005) and Zeinali and Notash (2010):

$$V(t) = \frac{1}{2} s^T B s + \frac{1}{2} \tilde{d}^T K_{is}^{-1} \tilde{d}, \tag{8}$$

where $\tilde{d}^{T}(t)$ is defined as the vector of the lumped uncertainty estimation error and is given by Zeinali and Notash (2010):

$$\tilde{d} = \hat{d} - d, \tag{9}$$

and here $\hat{d}$ is the estimated perturbation vector of the unknown actual perturbation vector d that is defined in Eq. (4).

The derivative of the Lyapunov function is:

$$V' = s^T B' s + \frac{1}{2} s^T B' s + \tilde{d}^{T} K_{is}^{-1} \overset{\sim}{d'}. \tag{10}$$

From Eq. (6), one can get:

$$s' = K_d e'' + K_p e' + K_i e. \tag{11}$$

Substitution of $e'' = q'' - q_d''$ in Eq. (11) yields:

$$s' = K_d \{q'' - q_d''\} + K_p e' + K_i e. \tag{12}$$

Then, by substituting for q'' from Eq. (5) one gets:

$$\tilde{s} = K_p e' + K_i e - K_d B^{-1} [q' + g - d] + K_d B^{-1} u - K_d q_d''. \tag{13}$$

Substitution of Eq. (13) into Eq. (10) leads to:

$$\begin{aligned} V' = {} & s^T B \left\{K_p e' + K_i e - K_d B^{-1} [q' + g - d] + K_d B^{-1} u - K_d q_d''\right\} \\ & + \tfrac{1}{2} s^T B'' s + \tilde{d}^{T} K_{is}^{-1} \overset{\sim}{d'}. \end{aligned} \tag{14}$$

Further, substitution of Eq. (7) into Eq. (14) gives:

$$\begin{aligned} & V' = s^T \times \\ & \left\{BK_p e' + BK_i e - BK_d B^{-1} [q' + g - d] + BK_d B^{-1} u_{PID} + BK_d B^{-1} u_{SSDCPI}\right\} \\ & - s^T BK_d q_d'' + \frac{1}{2} s^T B' s + \tilde{d}^{T} K_{is}^{-1} \overset{\sim}{d'}. \end{aligned} \tag{15}$$

Finally, by substituting $q' = e' + q_d'$ into Eq. (3) we obtain:

$$\begin{aligned} & V' = s^T \times \\ & \left\{BK_p e' + BK_i e - BK_d B^{-1} [C' e + g - d] + BK_d B^{-1} u_{PID} + BK_d B^{-1} u_{SSDCPI}\right\} \\ & - s^T BK_d B^{-1} C' q_d - s^T BK_d q_d'' + \frac{1}{2} s^T B' s + \sim d^T K_{is}^{-1} \overset{\sim}{d'}. \end{aligned} \tag{16}$$

The PID control law $u_{PID}(t)$ can be chosen as:

$$u_{PID}(t) = \\ -\left\{K_s + K_{p,PID}\ \|e(t)\| + K_{i,PID}\left\|\int e(\xi)d\xi\right\| + K_{d,PID}\,\|e'(t)\|\right\}\frac{s(t)}{\|s(t)\|}, \tag{17}$$

where K_s represents an $n \times n$ diagonal positive definite switching control gain matrix, $K_{p,PID}$is an $n \times n$ diagonal positive definite proportional gain matrix, $K_{i,PID}$is an $n \times n$ diagonal positive definite integral gain matrix, and $K_{d,PID}$ is an $n \times n$ diagonal positive definite derivative gain matrix. These matrices are design parameters to be selected.

The sliding surface dynamics based continuous proportional-integral (PI) control action, $u_{SSDCPI}(t, s)$, can be chosen as (see Zeinali and Notash, 2010):

$$u_{SSDCPI}(t) = -\left\{K_{ps}s(t) + \hat{d}\,(t)\right\}, \tag{18}$$

where K_{ps} is an $n \times n$ diagonal positive definite matrix that is a design parameter to be selected.

Now, by substituting Eq. (3) and Eq. (18) into Eq. (3) we arrive at:

$$\begin{aligned} V' &= s^T\left\{BK_pe' + BK_ie - BK_dB^{-1}\left[C'e + g - d\right]\right\} \\ &-s^T\left\{BK_dB^{-1}\left[K_s + K_{p,PID}\ \|e\| + K_{i,PID}\left\|\int e(\xi)d\xi\right\| + K_{d,PID}\,\|e'\|\right]\frac{s}{\|s\|}\right\} \\ &-s^TBK_dB^{-1}\left[K_{ps}s + \hat{d}\right] - s^TBK_dB^{-1}C'q_d - s^TBK_dc_d'' + \frac{1}{2}s^TB's + \tilde{d}^T\ K_{is}^{-1}\ \overset{\sim}{d'}. \end{aligned} \tag{19}$$

By using $s^Ts = \|s\|^2$, $K_d = k_dI$, $K_p = k_p\,I$, $K_i = k_iI$, $K_s = k_sI$, $K_{p,PID} = k_{p,PID}I$, $K_{i,PID} = k_{i,PID}I$, $K_{d,PID} = k_{d,PID}I$ and $K_{ps} = k_{ps}I$, where $I_{n\times n}$ denotes the identity matrix of dimension $n \times n$, Eq. (**??**) can be rearranged as:

$$\begin{aligned} V' = s^T\ &\{k_pB'e + k_iBe - k_dC'e - k_dg\} \\ &-k_d\left[k_s + k_{p,PID}\ \|e\| + \left[k_{i,PID}\left\|\textstyle\int ed\xi\right\| + k_{d,PID}\,\|e'\|\right]\right. \\ &\|s\| - k_dk_{ps}\,\|s\|^2 - k_ds^T\hat{d} + k_ds^Td \\ &-k_ds^TC'q_d - k_ds^TB''q_d + \tfrac{1}{2}s^T\left\{B' - 2C\right\}s\ + s^TC\,s + \tilde{d}^T\ K_{is}^{-1}\ \overset{\sim}{d'}\ . \end{aligned} \tag{20}$$

Since $(B' - 2C)$ is a skew symmetric matrix, Eq. (20) becomes:

$$\begin{aligned} V' = s^T\ &\{k_pB'e + k_iBe - k_dC'e - k_dg\} \\ &-k_d\left[k_s + k_{p,PID}\,\|e\| + k_{i,PID}\left\|\textstyle\int ed\xi\right\| + k_{d,PID}\,\|e'\|\right] \\ &\|s\| - k_dk_{ps}\,\|s\|^2 - k_ds^T\hat{d} + k_ds^Td \\ &-k_ds^TC'q_d - k_ds^TB''q_d + s^TCs + \tilde{d}^T\ K_{is}^{-1}\overset{\sim}{d'}. \end{aligned} \tag{21}$$

Substituting $s(t)$ from Eq. (6) into Eq. (21), with the help of $K_d = k_d I$, $K_i = k_i I$ and $K_p = k_p I$, and rearranging the result yields:

$$\begin{aligned} V' = s^T & \left\{k_p B' e + [k_i B + k_p C]\, e + k_i C \int e dt - k_d g\right\} \\ & -k_d \left[k_s + k_{p,PID} \left\|e\right\| + k_{i,PID} \left\|\int e d\xi\right\| + k_{d,PID} \left\|e'\right\|\right] \\ & \left\|s\right\| - k_d k_{ps} \left\|s\right\|^2 - k_d s^T C' q_d \\ & -k_d s^T B'' q_d - k_d s^T \left(\hat{d} - d\right) + \tilde{d}^T K_{is}^{-1} \overset{\sim}{d'}. \end{aligned} \tag{22}$$

By exploiting Eq. (9) with its first time derivative, and the facts that

$$\left(s^T \tilde{d} = \tilde{d}^T s\right) \text{ and } (K_{is} = k_{is}\, I)\,,$$

we will bring Eq. (22) to the form:

$$\begin{aligned} V' = s^T & \left\{k_p B' e + [k_i B + k_p C]\, e + k_i C \int e dt - k_d g\right\} \\ & -k_d \left[k_s + k_{p,PID} \left\|e\right\| + k_{i,PID} \left\|\int e d\xi\right\| + k_{d,PID} \left\|e'\right\|\right] \\ & \left\|s\right\| - k_d k_{ps} \left\|s\right\|^2 - k_d s^T C' q_d \\ & -k_d s^T B'' q_d - \tilde{d}^T \left\{k_d s - \tfrac{1}{k_{is}} \overset{\wedge}{d'}\right\} - \tfrac{1}{k_{is}} \tilde{d}^T d'. \end{aligned} \tag{23}$$

The first time derivative (dynamics) of the estimated uncertainty vector can be chosen as (see Zeinali and Notash, 2010):

$$\overset{\wedge}{d'}(t) = k_{is} k_d\, s(t). \tag{24}$$

Integration of Eq. (24) results in determination of the time evolution of the estimated uncertainty vector:

$$\hat{d} = k_{is} k_d \int s dt. \tag{25}$$

Substituting Eq. (24) into Eq. (23) leads to:

$$\begin{aligned} V' = s^T & \left\{k_p B' e + [k_i B + k_p C]\, e + k_i C \int e dt - k_d g\right\} \\ & -k_d \left[k_s + k_{p,PID} \left\|e\right\| + k_{i,PID} \left\|\int e d\xi\right\| + k_{d,PID} \left\|e'\right\|\right] \\ & \left\|s\right\| - k_d k_{ps} \left\|s\right\|^2 \\ & -k_d s^T C' q_d - k_d s^T B' q_d - \tfrac{1}{k_{is}} \overset{\sim}{d'}^T d'. \end{aligned} \tag{26}$$

By taking the norms of the different terms, Eq. (26) can be rewritten as:

$$\begin{aligned} V' \leq \left\|s\right\| & \left\{k_p \left\|B\right\| \left\|e'\right\| + (k_i \left\|B\right\| + k_p \left\|C\right\|) \left\|e\right\| + k_i \left\|C\right\| \left\|\int e dt\right\| + k_d \left\|g\right\|\right\} \\ & -k_d \left\{k_s + k_{p,PID} \left\|e\right\| + k_{i,PID} \left\|\int e(\xi) d\xi\right\| + k_{d,PID} \left\|e'\right\|\right\} \left\|s\right\| - k_d k_{ps} \left\|s\right\|^2 \\ & +k_d \left\|s\right\| \left\|C(q,q')\right\| \left\|q'_d\right\| + k_d \left\|s\right\| \left\|B\right\| \left\|q''_d\right\| - \frac{1}{k_{is}} \tilde{d}^T d'. \end{aligned} \tag{27}$$

Then, Eq. (3) can be rearranged to the following form:

$$\begin{aligned} V' \leq & -\|s\| \left\{ \left[k_d k_{d,PID} - k_p \|B\| \right] \|e'\| + \left[k_d k_{p,PID} - k_i \|B\| - k_p \|C\| \right] \|e\| \right. \\ & \left. + \left[k_d k_{i,PID} - k_i \|C\| \right] \left\| \int e dt \right\| + k_d \left[k_s - \|g\| - \|C\| \|q'_d\| - \|B\| \|q''_d\| \right] \right\} \\ & -k_d k_{ps} \|s\|^2 - \tfrac{1}{k_{is}} \tilde{d}^T d'. \end{aligned} \tag{28}$$

For the derivative of the Lyapunov function to be negative definite, $V' < 0$, the parameters of the proposed PID control action in Eq. (3) must satisfy the following stability conditions:

$$\begin{aligned} & k_{d,PID} \geq \tfrac{k_p \|B(q)\|}{k_d}, \qquad && k_{p,PID} \geq \tfrac{k_i \|B(q)\| + k_p \left\| C(q,q') \right\|}{k_d} \\ & k_{i,PID} \geq \tfrac{k_i \left\| C(q,q') \right\|}{k_d}, \qquad && k_s \geq \|g(q)\| + \|C(q,q')\| \|q'_d\| + \|B(q)\| \|q''_d\|. \end{aligned} \tag{29}$$

Substitution of Eq. (29) into Eq. (28) yields:

$$V' \leq -k_d k_{ps} \|s\|^2 - \frac{1}{k_{is}} \tilde{d}^T d'. \tag{30}$$

In Eq. (30), the first term is negative definite. If the perturbation vector $d(t)$ is slowly time-varying (Zeinali and Notash, 2010), which is a reasonable assumption in many control applications (i.e. $d'(t) \approx 0$ is negligible), then the second term $\left(k_{is}^{-1} \tilde{d}^T d' \approx 0 \right)$ is neglected, and therefore, it follows that $V'(t) < 0$ and the global asymptotic stability is guaranteed even if the perturbation vector $d(t)$ takes important values, as long as $d(t)$ is slowly time varying. The difficult situation is when the perturbation vector $d(t)$ is quickly time-varying (see Zeinali and Notash, 2010), i.e. $d'(t) \neq 0$. In this case, the sufficient condition $k_{is}^{-1} \tilde{d}^T d'(t) > 0$ ensures that the asymptotic stability is guaranteed and $V'(t) < 0$. Also, for a proper selection of the parameter values for the perturbation estimator in Eq. (25), (k_d, k_{is}), the estimation error vector $\tilde{d}^T$ is very small and converges to zero $\left(\tilde{d}^T \to 0 \right)$. Therefore, $V'(t) < 0$ and asymptotic stability is achieved. From the above analysis, it can be concluded that global asymptotic stability is guaranteed since the derivative of the Lyapunov function is negative definite, $V'(t) < 0$.

Based on Eqs. (7), (3), (3) and (25), the total proposed PID sliding mode control algorithm with sliding surface dynamics-based continuous proportional-integral (PI) control action (PIDSMC-SSDCPI) can be expressed as:

$$u(t,s) = u_{PID}(t) + u_{SSDCPI}(t,s)$$

$$u_{PID}(t) = -\left\{K_s + K_{p,PID}\ \|e(t)\| + K_{i,PID}\left\|\int e(\xi)d\xi\right\| + K_{d,PID}\,\|e'(t)\|\right\}\frac{s(t)}{\|s(t)\|}$$

$$u_{SSDCPI}(t) = -\left\{K_{ps}s(t) + \hat{d}\ (t)\right\} = -\left\{K_{ps}s(t) + \underbrace{k_{is}k_d\int s(t)dt}_{\hat{d}(t)}\right\}$$

$$u(t,s) = -\underbrace{\left[\left\{K_s + K_{p,PID}\ \|e(t)\| + K_{i,PID}\left\|\int e(\xi)d\xi\right\| + K_{d,PID}\,\|e'(t)\|\right\}\frac{s(t)}{\|s(t)\|}\right]}_{u_{PID}(t)}$$
$$-\underbrace{\left[\left\{K_{ps}s(t) + k_{is}k_d\int s(t)dt\right\}\right]}_{u_{SSDCPI}(t,s)}. \tag{31}$$

The block diagram of the proposed PID sliding mode controller algorithm with sliding surface dynamics based continuous proportional-integral (PI) control action (PIDSMC-SSDCPI) is shown in Fig. 1.

4. ANFIS-based PID continuous sliding mode controller

Since the operating conditions of the robot manipulators tend to vary a lot, the design of a robust controller to work under a wide range of operating conditions has been given a great attention with the aim to enhance the closed-loop control system tracking performance. In this section, an adaptive neuro-fuzzy inference system (ANFIS) based-PID continuous sliding mode control algorithm (ANFIS-PIDCSMC) is adopted, in which the sliding surface dynamics-based continuous proportional-integral (SSDCPI) control action, $u_{SSDCPI}(t,s)$, realized with the presented PIDSMC-SSDCPI control methodology is supplanted by ANFIS control action $u_{ANFIS}(t)$.

Integration of the ANFIS technique as an intelligent and soft computing methodology (Alavandar and Nigam, 2009c; Zeinali and Notash, 2010) with the PID sliding mode control scheme secures fast tracking control behavior and improves the robot system robustness. The ANFIS-PIDCSMC controller can

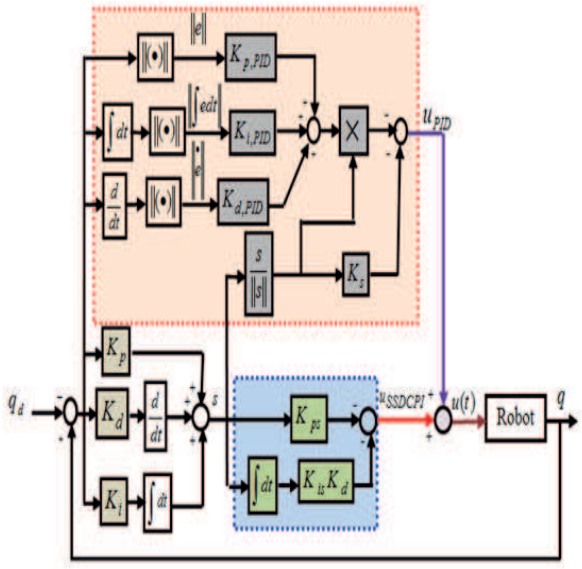

Figure 1. Block diagram of the PID sliding mode controller with continuous proportional-integral (PI) control action

be expressed as:

$$u(t) = u_{PID}(t) + u_{ANFIS}(t)$$
$$u(t) = -\left\{K_s + K_{p,PID}\,\|e(t)\| + K_{i,PID}\left\|\int e(\xi)d\xi\right\| + K_{d,PID}\,\|e'(t)\|\right\} \frac{s(t)}{\|s(t)\|} + u_{ANFIS}(t). \tag{32}$$

The schematic diagram of the ANFIS-PIDCSMC controller is provided in Fig. 2.

The ANFIS approach (see Alavandar and Nigam, 2009c; Kar, Das and Ghosh, 2014) uses a hybrid learning algorithm to identify parameters of Sugeno-type fuzzy inference systems. It applies a combination of the least-squares method and the backpropagation gradient descent method for training the membership function (MF) parameters to emulate a given training data set (see Buragohain and Mahanta, 2008; Alavandar and Nigam, 2009c; Aloui et al., 2010; and Bhattacharyya et al., 2015). In the architecture of the ANFIS configuration, a first-order Takagi–Sugeno–Kang (TSK) fuzzy inference system is

exploited with fuzzy IF-THEN rules that can be expressed as:

$$\begin{array}{l} Rule\,1: If\ (s)\ is\ A_1\ and\ \left(\int sdt\right)\ is\ B_1\ \ then\ \ z_1 = a_1(s) + b_1\left(\int sdt\right) + c_1 \\ Rule\,2: If\ (s)\ is\ A_2\ and\ \left(\int sdt\right)\ is\ B_2\ \ then\ \ z_2 = a_2(s) + b_2\left(\int sdt\right) + c_2 \\ \qquad\qquad\qquad\qquad \vdots \\ \qquad\qquad\qquad\qquad \vdots \\ \qquad\qquad\qquad\qquad \vdots \\ Rule\,n: If\ (s)\ is\ A_{m_1}\ and\ \left(\int sdt\right)\ is\ B_{m_2}\ then\ \ z_n = a_n(s) + b_n\left(\int sdt\right) + c_n \end{array} \tag{33}$$

where $A_1,\ A_2 \ldots A_{m_1}$ and $B_1, B_2 \ldots B_{m_2}$ are the fuzzy sets (membership functions) in the antecedent defined for the two inputs (s) and $\left(\int sdt\right)$, respectively, where m_1 and m_2 are the numbers of membership functions assigned to the two inputs (s) and $\left(\int sdt\right)$, respectively. The parameters $a_1,\ a_2 \ldots a_n,\ b_1,\ b_2 \ldots b_n$ and $c_1, c_2 \ldots c_n$ are the consequent parameters that are the design parameters to be determined during the training process, where n represents the number of fuzzy rules. The general ANFIS architecture is shown in Fig. 2 for the case of two fuzzy rules. It is composed of five layers, where each layer contains several nodes, described by the node function such that O_i^j is the output of the node i in layer j.

In Fig. 2, a circle indicates a fixed node and a square represents an adaptive node. The function of each layer is explained as follows (see Mozaffari, Behzadipour and Kohani, 2014; Alavandar and Nigam, 2009c; Bhattacharyya et al., 2015; and Sumathis and Surekha, 2010):

Layer 1 (Fuzzy layer): in the first layer, all the nodes are adaptive nodes. The outputs of layer 1 are the fuzzy membership grades of the inputs, which are given by (see Su and Leung, 1993):

$$\begin{array}{ll} O_i^1 = \mu_{A_i}(s), & i = 1,\ 2 \\ O_i^1 = \mu_{B_{i-2}}\left(\int sdt\right), & i = 3,\ 4 \end{array} \tag{34}$$

where A_i and B_i are the linguistic labels (fuzzy sets or membership functions) of the inputs (s) and $\left(\int sdt\right)$, respectively. $\mu_{A_i}(s)$ and $\mu_{B_{i-2}}\left(\int sdt\right)$ are the grades (degrees) of membership for the inputs (s) and $\left(\int sdt\right)$, respectively. The outputs of this layer form the membership values of the premise part and parameters contained in membership functions of fuzzy sets called premise parameters. The $\mu_{A_i}(s)$ and $\mu_{B_{i-2}}\left(\int sdt\right)$ are chosen as Gaussian membership functions (Sumathi and Surekha, 2010):

$$\begin{array}{l} \mu_{A_i}(s) = \exp\left[-\left(\frac{s - c_{Ai}}{\sigma_{Ai}}\right)^2\right] \\ \mu_{B_{i-2}}\left(\int sdt\right) = \exp\left[-\left(\frac{\left(\int sdt\right) - c_{Bi}}{\sigma_{Bi}}\right)^2\right]. \end{array} \tag{35}$$

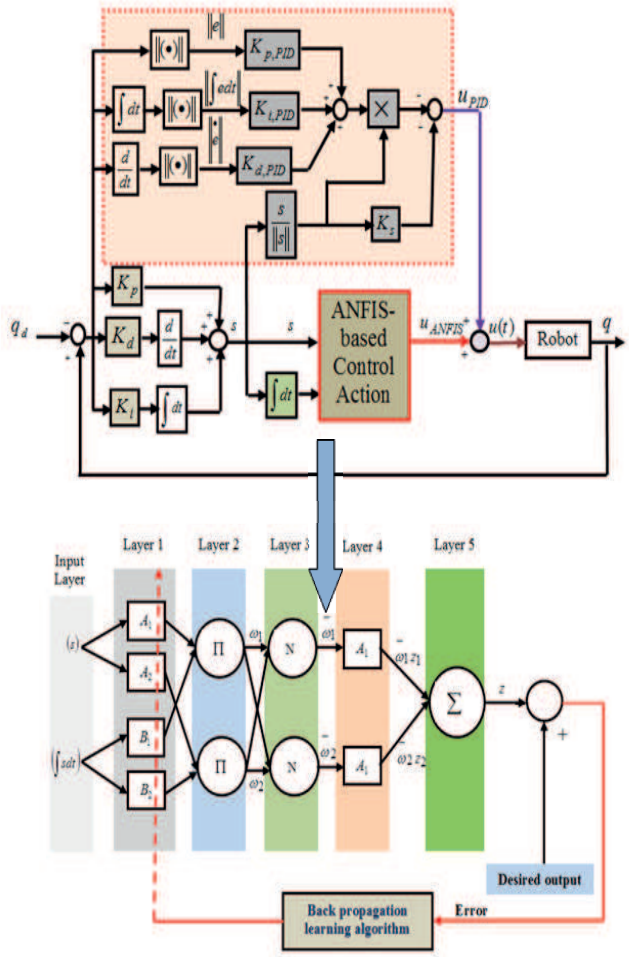

Figure 2. Block diagram of the ANFIS-based PID sliding mode controller

where $\{c_{Ai},\, \sigma_{Ai},\, c_{Bi},\, \sigma_{Bi}\}$ is the variable set of the membership functions. These parameters are called premise variables.

Layer 2 (Product layer): in the second layer, every node is a fixed node, labeled (Π), acting as a simple multiplier. The outputs of these nodes, which are called the firing strengths of the fuzzy rules, are given by (see Mozaffari, Behzadipour and Kohani, 2014; Bhattacharyya et al., 2015; Sumathi and Surekha, 2010):

$$\omega_i = O_i^2 = \mu_{A_i}(s) \times \mu_{B_i}\left(\int sdt\right) \qquad i = 1,\, 2. \tag{36}$$

Layer 3 (Normalized layer): in the third layer, every node is a fixed node, labeled N, calculating the normalized firing strengths as the ratio of the firing strength of node i to the sum of the firing strengths of all fuzzy rules. The outputs of these nodes, which are called the normalized firing strengths, are given by (see Alavandar and Nigam, 2009c; Bhattacharyya et al., 2015; Sumathi and Surekha, 2010):

$$O_i^3 = \overline{\omega_i} = \frac{\omega_i}{\omega_1 + \omega_2} = \frac{\omega_i}{\sum\limits_{i=1}^{2} \omega_i} \qquad i = 1,\, 2. \tag{37}$$

Layer 4 (Defuzzification layer): in the fourth layer, every node is an adaptive node, which calculates the outputs of the fuzzy rules as (see Bhattacharyya et al., 2015; Sumathi and Surekha, 2010):

$$O_i^4 = \overline{\omega_i}\, z_i \,=\, \overline{\omega_i}\left(a_i\, s \,+\, b_i\left(\int sdt\right) \,+\, c_i\right) \qquad i = 1,\, 2. \tag{38}$$

where $\{a_i,\, b_i,\, c_i\}$ constitutes the parameter set. Parameters in this layer are referred to as consequent parameters.

Layer 5 (Output layer): In the fifth layer, there is a single fixed node, labeled $(\sum)$, which calculates the overall output as the sum of all incoming signals that is given by (see Bhattacharyya et al., 2015; Sumathi and Surekha, 2010):

$$O_i^5 = \sum_{i=1}^{2} \overline{\omega_i}\, z_i = \overline{\omega_1}\, z_1 + \overline{\omega_2}\, z_2 = \left(\frac{\omega_1 z_1}{\sum\limits_{i=1}^{2} \omega_i}\right) + \left(\frac{\omega_2 z_2}{\sum\limits_{i=1}^{2} \omega_i}\right) = \frac{\sum\limits_{i=1}^{2} \omega_i z_i}{\sum\limits_{i=1}^{2} \omega_i}. \tag{39}$$

From the above explanation of the five layers, illustrated in Fig. 2, it is clear that an ANFIS is a kind of fuzzy model, in which a feed-forward neural network

is used for the weighted value evaluation of fuzzy rules (Angeles, 2003; Choi and Cheol Lee, 2009). In ANFIS, a feed-forward back-propagation algorithm tunes the parameters of the fuzzy inference system (FIS), such as membership functions parameters of the antecedent part and consequent parameters, by applying neural learning rules (Angeles, 2003; Choi and Cheol Lee, 2009). It can be seen that there are two modifiable parameter sets, namely: $\{c_{Ai}, \sigma_{Ai}, c_{Bi}, \sigma_{Bi}\}$, labeled as premise parameters, and $\{a_i, b_i, c_i\}$, labeled as consequent parameters. The aim of the training algorithm for this architecture is to tune the above two parameter sets to make the ANFIS output match the training data (Mozaffari, Behzadipour and Kohani, 2014).

5. Simulation results

To verify the validity of the proposed control strategy, the ANFIS-PIDCSMC control approach is tested for the trajectory tracking control of a rigid robot manipulator (RRM), see Elmali and Olgac (1992), shown in Fig. 3. In this validation, numerical simulations, which are performed in the case of high speed motion and the case of a pick-and-place task, are presented to show the effectiveness of the proposed approach. The simulations are carried out using the Simulink software library of the MATLAB programming language. For comparison, the traditional sliding mode controller (TSMC) and the standalone PID controller are used.

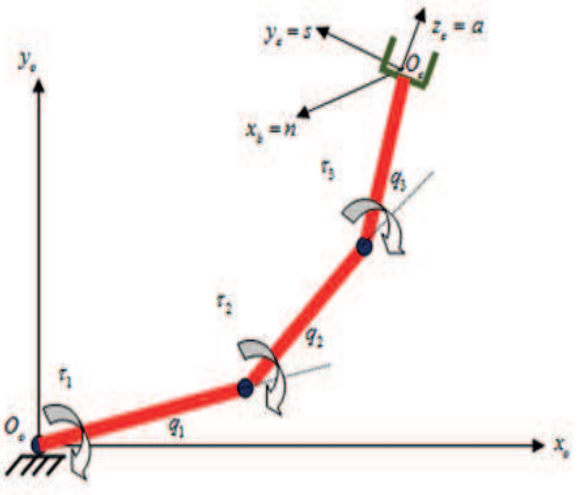

Figure 3. Three-link rigid robot manipulator

The RRM is described by three nonlinear coupled differential equations

representing the dynamical model (see Elmali and Olgac, 1992), namely:

$$\{I_{l1} + m_{l1}l_1^2 + k_{r1}^2 I_{m1} + I_{l2} + m_{m2}a_1^2 + I_{m2} + m_{l2}(a_1^2 + l_2^2 + 2a_1 l_2 c_2) + I_{l3}$$
$$+I_{m3} + m_{m3}(a_1^2 + a_2^2 + 2a_1 a_2 c_1) + m_{l3}(a_1^2 + a_2^2 + l_3^2 + 2a_1 a_2 c_2 + 2a_1 l_3 c_{23}$$
$$+2a_2 l_3 c_3)\}q_1'' + \{I_{l2} + I_{l3} + k_{r2}I_{m2} + I_{m3} + m_{m3}a_2^2 c_2 + m_{l2}(a_2^2 + a_1 a_2 c_2)$$
$$+m_{l3}(a_2^2 + l_3^2 + a_1 a_2 c_2 + a_1 l_3 c_{23} + 2a_2 l_3 c_3)\}q_2'' + \{I_{l3} + k_{r3}I_{m3} + m_{l3}(l_3^2$$
$$+a_1 l_3 c_{23} + a_2 l_3 c_3)\}q_3'' - m_{m3}a_1 a_2 s_1 {q'}_1^2 - 2(m_{l2}a_1 l_2 s_2 + m_{l3}a_1 a_2 s_2$$
$$+m_{l3}a_1 l_3 s_{23})q_1' q_2' - 2(m_{l3}a_1 l_3 s_{23} + m_{l3}a_2 l_3 s_3){q'}_1 q_3' - (m_{l3}a_1 a_2 s_2$$
$$+m_{l3}a_1 l_3 s_{23} + m_{m3}a_1 a_2 s_2 + m_{l2}a_1 a_2 s_2){q'}_2^2 - 2(m_{l3}a_1 l_3 s_{23} + m_{l3}a_2 l_3 s_3)q_2' q_3'$$
$$-(m_{l3}a_2 l_3 s_2 + m_{l3}a_1 l_3 s_{23}){q'}_3^2 + (m_{l1}l_1 + m_{l2}a_1 + m_{m2}a_1 + m_{l3}a_1 + m_{m3}a_1)gc_1$$
$$+(m_{l2}l_2 + m_{l3}a_2 + m_{m3}a_2)gc_{12} + m_{l3}l_3 gc_{123} = \tau_1 \tag{40}$$

$$\{I_{l2} + I_{l3} + k_{r2}I_{m2} + I_{m3} + m_{m3}a_2^2 c_2 + m_{l2}(a_2^2 + a_1 a_2 c_2) + m_{l3}(a_2^2 + l_3^2$$
$$+a_1 a_2 c_2 + a_1 l_3 c_{23} + 2a_2 l_3 c_3)\}q_1'' + \{I_{l2} + I_{l3} + k_{r2}^2 I_{m2} + m_{m3}a_2^2 + m_{l2}a_2^2$$
$$+m_{l3}(a_2^2 + l_3^2 + 2a_2 l_3 c_3)\}q_2'' + \{I_{l3} + k_{r3}I_{m3} + m_{l3}(l_3^2 + a_2 l_3 c_3)\}q_3''$$
$$+\{m_{l2}a_1 l_2 s_2 + m_{l3}a_1 a_2 s_2 + m_{l3}a_1 l_3 s_{23}\}{q'}_1^2 - 2(m_{l3}a_2 l_3 s_3)q_1' q_3' - 2(m_{l3}a_2$$
$$l_3 s_3)q_2' q_3' - (m_{l3}a_2 l_3 s_3){q'}_3^2 + (m_{l2}l_2 + m_{l3}a_2 + m_{m3}a_2)gc_{12} + m_{l3}l_3 gc_{123} = \tau_2 \tag{41}$$

$$\{I_{l3} + k_{r3}I_{m3} + m_{l3}(l_3^2 + a_1 l_3 c_{23} + a_2 l_3 c_3)\}q_1'' + \{I_{l3} + k_{r3}I_{m3} + m_{l3}(l_3^2$$
$$+a_2 l_3 c_3)\}q_2'' + \{I_{l3} + k_{r3}^2 I_{m3} + m_{l3}l_3^2\}q_3'' + \{m_{l3}a_1 l_3 s_{23} + m_{l3}a_2 l_3 s_3\}{q'}_1^2$$
$$+2(m_{l3}a_2 l_3 s_3)q_1' q_2' + (m_{l3}a_2 l_3 s_3){q'}_2^2 - (m_{l3}a_2 l_3 s_3)q_2' q_3' + m_{l3}l_3 gc_{123} = \tau_3 \tag{42}$$

where $l_1 = l_2 = l_3 = 0.5$ m represent the distances of the centers of masses of the three links from the respective joint axes, $a_1 = a_2 = a_3 = 1.0$ m represent

the length of the three links, $m_{l1} = m_{l2} = m_{l3} = 10$ Kg are the masses of the three links, $m_{m1} = m_{m2} = m_{m3} = 1$ Kg are the masses of the rotors, $I_{l1} = I_{l2} = I_{l3} = 1.0$ Kg.m^2 are the moments of inertia of links and $I_{m1} = I_{m2} = I_{m3} = 0.01\,Kg.m^2$ are the moments of inertia of rotors. The cosines and sines of the joint angles are represented as:

$$\begin{array}{lll} c_1 = \cos q_1 & c_{12} = \cos(q_1 + q_2) & c_{123} = \cos(q_1 + q_2 + q_3) \\ s_1 = \sin q_1 & s_{12} = \sin(q_1 + q_2) & s_{123} = \sin(q_1 + q_2 + q_3). \end{array} \tag{43}$$

5.1. Tracking control of high speed trajectory

The desired trajectory, is assigned to the three joints of the robot arm and is given as:

$$q_d(t) = 1.5\,\{1 - \cos(1.5\,\pi\,t) + \sin(1.5\,\pi\,t)\}\,. \tag{44}$$

The initial posture of manipulator is assumed to be at $q(0) = [\pi\ \ \pi\ \ \pi]^T$ rad.

In order to check the robustness of the proposed controller (ANFIS-PIDCSMC), large severe uncertainties are simulated representing:

1. A step disturbance torque of $500\,N.m$, which is suddenly applied at the three joints at $t = 1.5$ sec., and is shown in Fig. 4.
2. An unpredicted variation at the mass and inertia of the third link of the robot occurs at $t = 1.5$ sec. The abrupt change of the mass m_{l3} and the inertia I_{l3} is shown in Fig. 5.
3. The nonlinear dynamic effects as viscous and static frictions are given by:

$$F_d\,q' = \begin{bmatrix} 5\,q'_1 \\ 5\,q'_2 \\ 5\,q'_3 \end{bmatrix}, \qquad F_s\,(q') = \begin{bmatrix} 5sign(q'_1) \\ 5sign(q'_2) \\ 5sign(q'_3) \end{bmatrix},$$
$$\tau_d = \begin{bmatrix} 500 + 500\sin(2t) + 500\cos(\frac{\pi}{2}t) \\ 500 + 500\sin(2t) + 500\cos(\frac{\pi}{2}t) \\ 500 + 500\sin(2t) + 500\cos(\frac{\pi}{2}t) \end{bmatrix}. \tag{45}$$

4. Also, the normally distributed noise affects the robot as disturbing torque acting on the three joints, as it is shown in Fig. 6.

The parameters of the standalone conventional PID controller are set as: $(K)_{PID} = diag\,\{22000, 10000, 20000\}$. The parameters of the TSMC are set as: the hitting control gain $K_r = diag\,\{12000, 12000, 12000\}$ and the slope of the sliding surface is $\lambda = diag\,\{3.5, 3.5, 3.5\}$. For the PIDSMC-SSDCPI controller, the relay gain k_s, the proportional gain $k_{p,\,PID}$, the integral gain $k_{i,\,PID}$ and the derivative gain $k_{d,\,PID}$ are set to satisfy the stability conditions in Eq. (29). The proportional gain is set as: $k_{p,\,PID} = 72000$, the integral gain is set as: $k_{i,\,PID} = 75000$, the derivative gain is set as: $k_{d,\,PID} = 50000$, and $k_s = 5500$. The sliding surface parameters are set as: $K_d = I_{3\times3}$, $K_p = diag\{10, 10, 10\}$

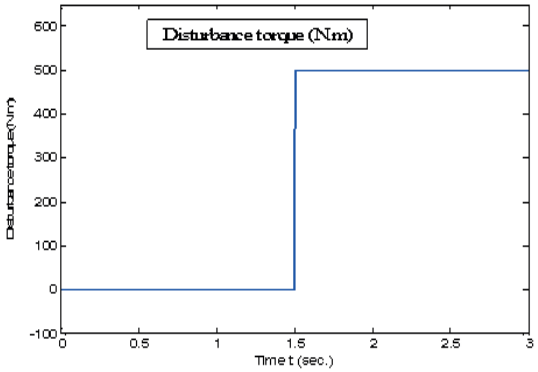

Figure 4. External disturbance torque (N. m)

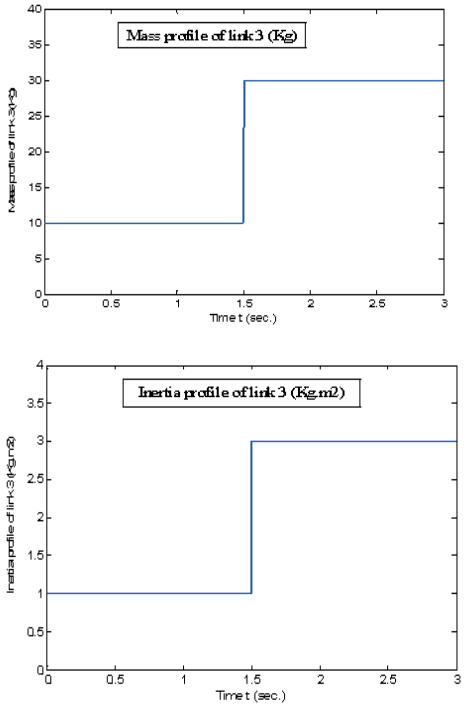

Figure 5. (a) Mass of link 3, (b) Moment of inertia of link 3. Variations of physical parameters of the third link

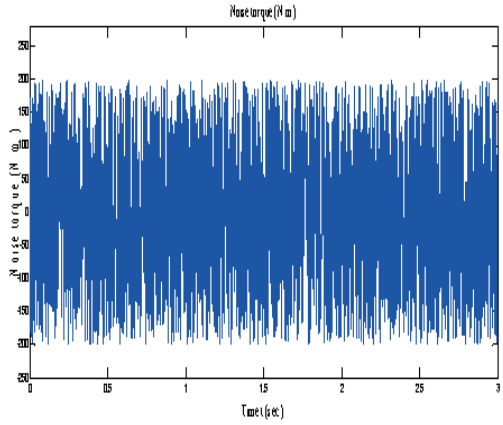

Figure 6. Normally distributed noise acting on the three joints

and $K_i = diag\{25, 25, 25\}$.

The training data set for the ANFIS controller is derived by performing computer simulations using the PIDSMC-SSDCPI controller as shown in Fig. 7, representing the block diagram simulated on the computer using the Simulink software library of the MATLAB programming language. The collected data is then used to train the ANFIS controller.

Figures 8, 9 and 10 show the positions of the three joints, 1, 2 and 3, respectively. The tracking position error profiles for joints 1, 2, and 3 are depicted in Figures 11, 12 and 13, respectively. It can be observed on the basis of these results that the ANFIS-PIDCSMC gives smaller tracking error, fast error convergence and better tracking performance than TSMC and PID controllers. It is seen that not only are there no chattering phenomena but also good robust trajectory tracking can be obtained in the conditions of parameter variations and external disturbance.

The time history of the sliding surface $s(t)$ is depicted in Figs. 14, 15 and 16 for the three joints 1, 2 and 3, respectively. The reaching phase, in which $s(t) \neq 0$, exists up to 0.15 sec., which means that the reaching time is 0.15 sec. The sliding mode, in which $s(t) = 0$, starts at 0.15 sec., where the error signal arrives at the sliding surface. Figures 17, 18 and 19 depict the total control signal of the all types of the used controllers for joint 1, joint 2 and joint 3, respectively.

Table 1 further on shows that the proposed approach has smaller error values than TSMC and PID controllers. The performance indices were calculated for each of the competing controllers for each joint as:

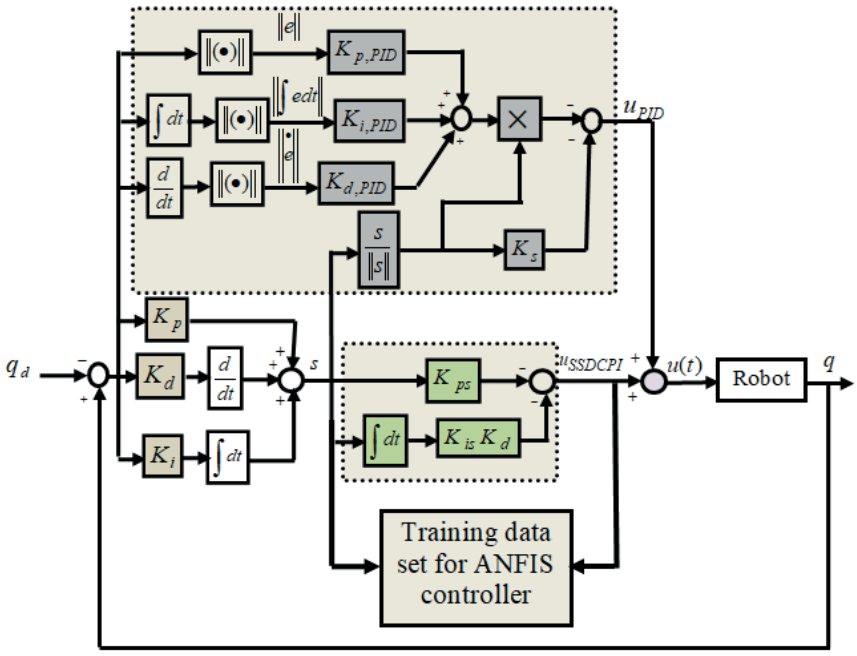

Figure 7. Simulated control system used to obtain the training data set for the ANFIS control term in ANFIS-PIDCSMC controller

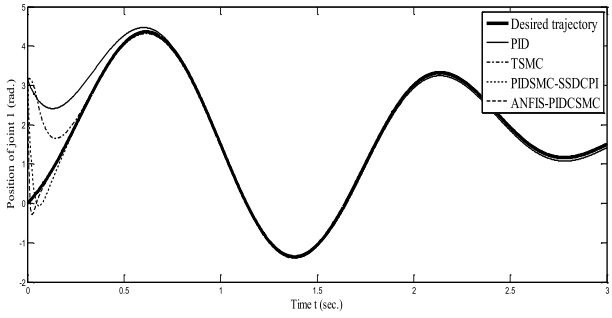

Figure 8. Position trajectory of joint 1

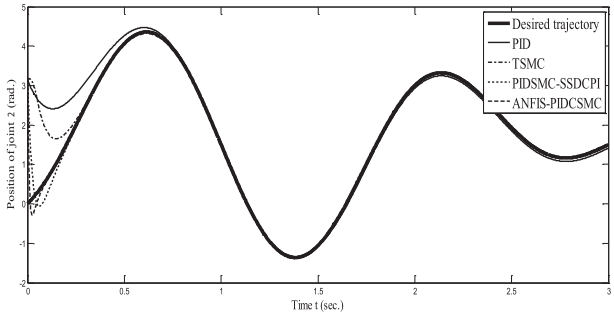

Figure 9. Position trajectory of joint 2

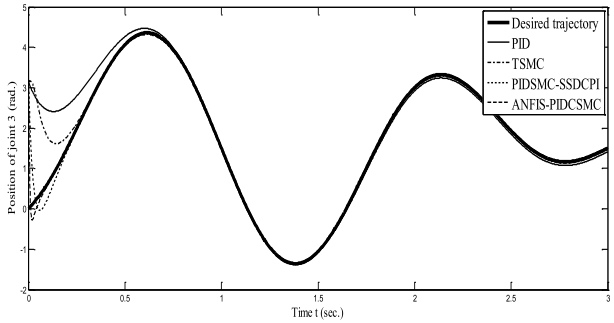

Figure 10. Position trajectory of joint 3

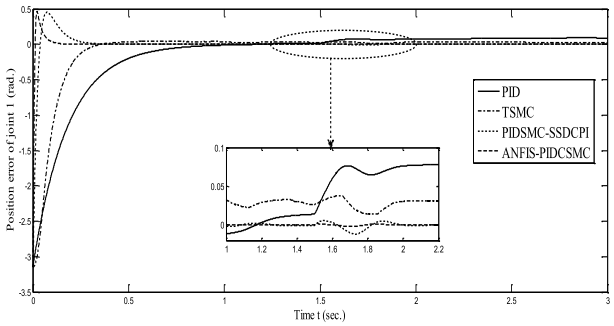

Figure 11. Position error of joint 1

Integral of absolute error:

$$IAE = \int |e(t)|\, dt. \tag{46}$$

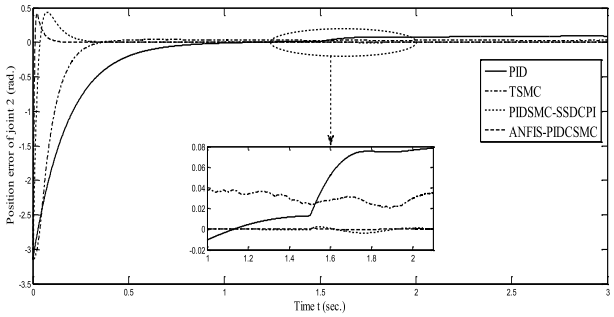

Figure 12. Position error of joint 2

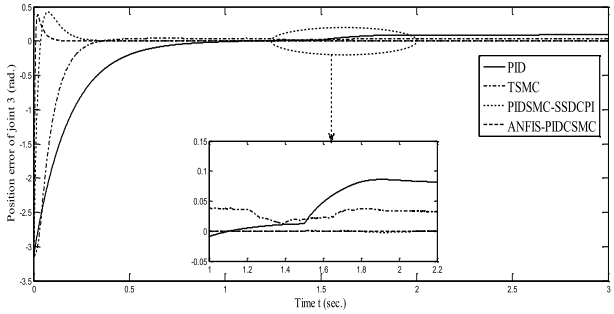

Figure 13. Position error of joint 3

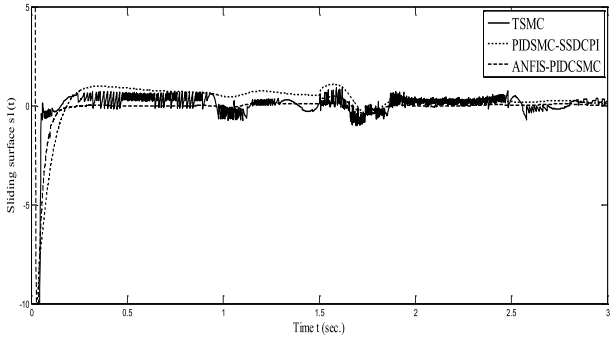

Figure 14. Trajectory of sliding surface for joint 1

Integral of time multiplied absolute error:

$$ITAE = \int t\,|e(t)|\,dt. \tag{47}$$

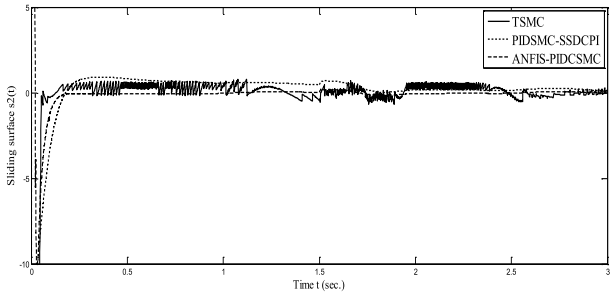

Figure 15. Trajectory of sliding surface for joint 2

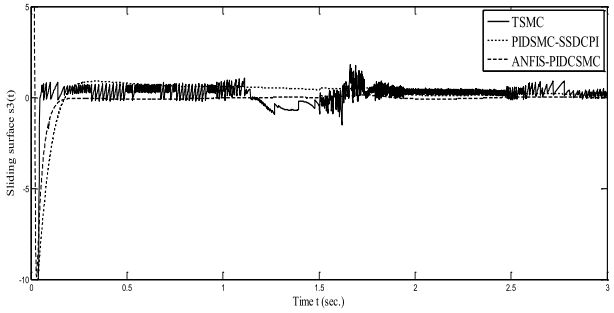

Figure 16. Trajectory of sliding surface for joint 3

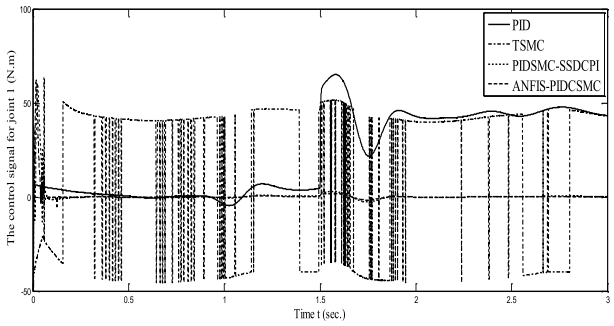

Figure 17. The total control signal of the all types of the used controllers for joint 1

The conclusion is that for our proposed approach both (IAE) and (ITAE), for the three joints, are considerably reduced in magnitude with regard to the other conventional methods referred to in this study.

Comparison between the trajectory tracking position errors obtained by the

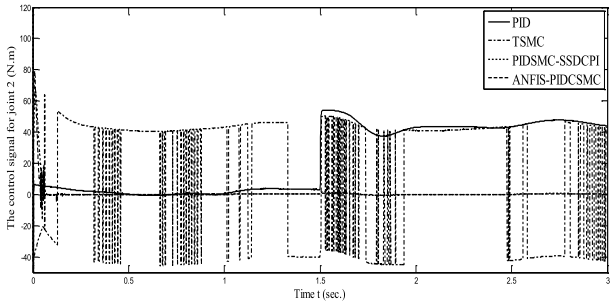

Figure 18. The total control signal of the all types of the used controllers for joint 2

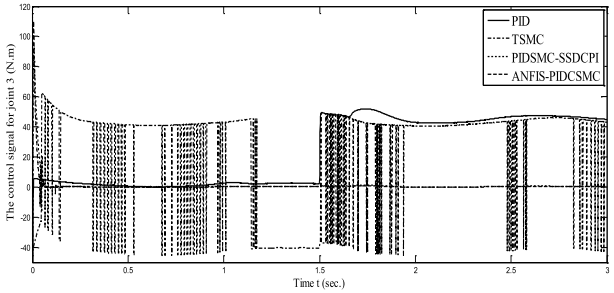

Figure 19. The total control signal of the all types of the used controllers for joint 3

Table 1. Performance comparison of the controllers

Algorithm	**IAE**			**ITAE**		
	Joint 1	**Joint 2**	**Joint 3**	**Joint 1**	**Joint 2**	**Joint 3**
PID	40.44	39.14	40.07	95.02	97.46	95.24
TSMC	29.98	31.12	30.27	41.77	42.87	40.21
PIDSMC-SSDCPI	15.12	14.87	15.79	39.95	38.40	37.43
ANFIS-PIDCSMC	6.49	7.25	5.27	26.98	24.50	25.42

proposed ANFIS-PIDCSMC controller and the tracking errors of the TSMC and PID controllers demonstrates that the ANFIS-PIDCSMC controller can achieve favorable and satisfying trajectory tracking control performance. Also, comparison results show that the proposed ANFIS-PIDCSMC control methodology

is able to control perfectly rigid robot manipulators and has excellent robustness performance, even when the closed-loop robot control system is subject to external disturbances and uncertainties.

5.2. Pick-in-place task

The desired joint angle function is chosen as:

$$q_d(t) = 2 + (-1 + \tanh(10\cos(0.25\,t))). \tag{48}$$

This function corresponds to the pick-in-place type task that is widely used in industrial applications. The desired trajectory is shown in Fig. 20. The uncertainty, external disturbance and the parameter variations are all applied at $t = 4.0$ sec.

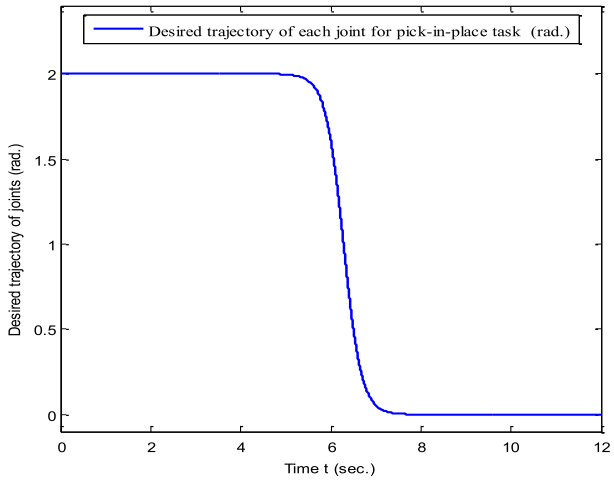

Figure 20. Desired trajectory for the pick-in-place task

Figures 21, 22 and 23 show the position of the three joints 1, 2 and 3, respectively. The tracking position error profiles for joints 1, 2, and 3 are depicted in Figs. 24, 25 and 26, respectively. Simulation results show that the proposed approach achieves better tracking response, faster rise time, faster settling time, less overshoot and lack of the steady state error, when compared to the traditional controllers, TSMC and PID. The values of different errors considered are provided in Table 2.

6. Conclusions

The present paper has described the development of an ANFIS-PIDCSMC control strategy. In the first design phase, a hybrid control scheme is developed,

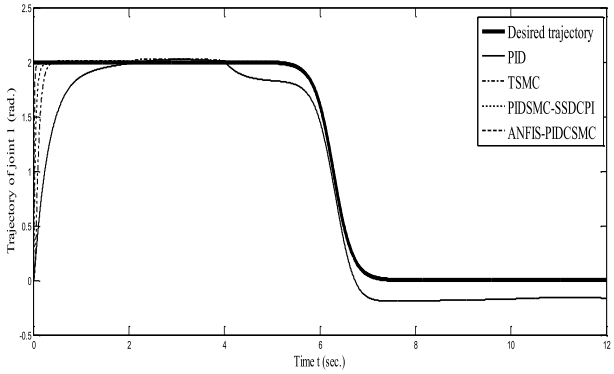

Figure 21. Position of joint 1 in the pick and place task

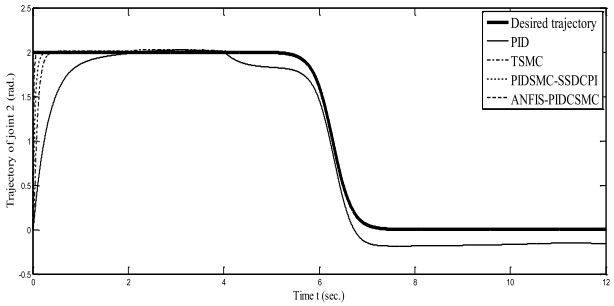

Figure 22. Position of joint 2 in the pick and place task

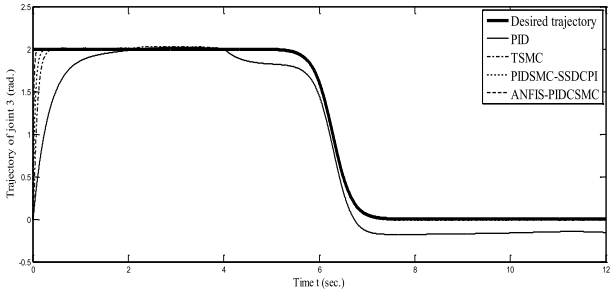

Figure 23. Position of joint 3 in the pick and place task

in which PIDSMC-SSDCPI controller is designed in such a way that the equivalent control term of the TSMC is replaced by PID controller with feedback relay control action (Jakarov, Parlakçi and Istefanopoulos, 2005) and the discontinuous control signal of the TSMC is replaced by the SSDCPI control action

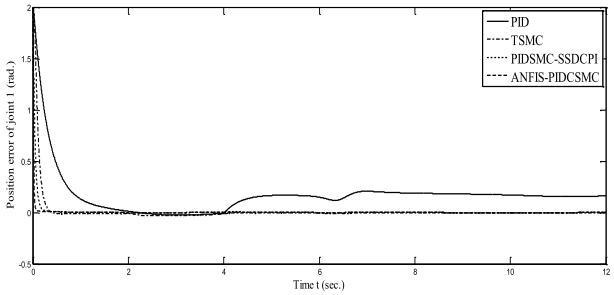

Figure 24. Position error of joint 1 in the pick and place task

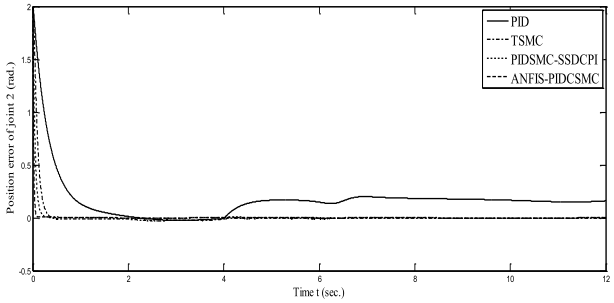

Figure 25. Position error of joint 2 in the pick and place task

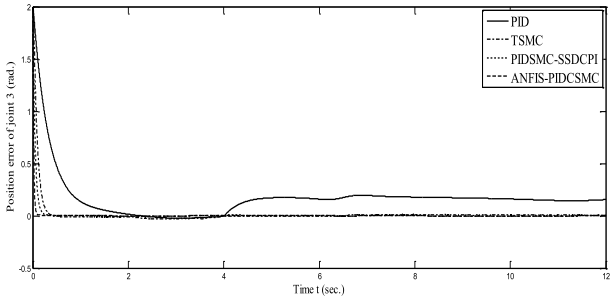

Figure 26. Position error of joint 3 in the pick- place task

(Zeinali and Notash, 2010). The overall closed-loop control system guarantees the global asymptotic stability of the closed-loop control system in terms of Lyapunov quadratic form.

In the second design stage, an ANFIS-PIDCSMC controller is introduced to increase the control system robustness against un-modeled dynamics (unstructured uncertainty), physical parameters variation (structured uncertainty)

Table 2. Performance comparison of the controllers for the pick and place task

Algorithm	**IAE** $\times 10^3$			**ITAE** $\times 10^3$		
	Joint 1	**Joint 2**	**Joint 3**	**Joint 1**	**Joint 2**	**Joint 3**
PID	2.0733	2.063	2.0547	11.087	10.947	10.782
TSMC	1.31	1.2352	1.3853	6.8272	6.728	8.296
PIDSMC-SSDCPI	0.4761	0.4579	0.4756	0.5369	0.5305	0.5221
ANFIS-PIDCSMC	0.3485	0.3485	0.3482	0.2261	0.2216	0.2159

and external disturbances. In designing the ANFIS-PIDCSMC controller, the PI control action in the PIDSMC-SSDCPI controller is replaced by an ANFIS control signal (Alavandar and Nigam, 2009c) such that the advantages of both artificial neural networks (ANNs) and fuzzy logic controllers (FLCs) have been utilized simultaneously.

For the proposed control algorithm, numerical simulations using the dynamic model of RRM with uncertainties and external disturbances show the excellent and effective performance of the adopted control approach in high-speed trajectory tracking control problems. The simulation results, compared with the results obtained with traditional controllers (standalone PID and TSMC), illustrate the fact that the tracking control behavior of the robot system displays better tracking performance than that of the conventional controllers.

References

Mozaffari, A., Behzadipour, S. and Kohani M. (2014) Identifying the tool-tissue force in robotic laparoscopic surgery using neuro-evolutionary fuzzy systems and a synchronous self-learninghyper level supervisor. *Applied Soft Computing*, **14**, 12–30.

Abdallah, B., Dawson, D., Dorato, P. and Jamshidi, M. (1991) Survey of robust control for rigid robots. *IEEE Control Systems Magazine*, **11**, 2, 24–30.

Alavandar, S. and Nigam, M. J. (2009a) Comparative Analysis of Conventional and Soft Computing Based Control Strategies for Robot Manipulators with Uncertainties. *International Journal of Computational Cognition*, **7**, 1, 52-61.

Alavandar, S. and Nigam, M. J. (2009b) New Hybrid Adaptive Neuro Fuzzy Algorithms for Manipulator Control with Uncertainties – Comparative Study. *ISA Trans.*, **48**, 4, 497-502.

Alavandar, S. and Nigam, M. (2009c) New hybrid adaptive neuro-fuzzy algorithms for manipulator control with uncertainties - Comparative study.

ISA Transactions, **48**, 4, 497-502.

Aloui, S., Pagès, O., El Hajjaji, A., Chaari, A. and Koubaa, Y. (2010) Improved fuzzy sliding mode control for a class of MIMO nonlinear uncertain and perturbed systems. *Applied Soft Computing*, **11**, 1, 820-826.

Angeles, I. (2003) *Fundamentals of Robotic Mechanical Systems*, second edition. Springer-Verlag, New York.

Barambones, O. and Etxebarria, V. (2000) Robust adaptive control for robot manipulator with un-modeled dynamics. *Int. J. Cybernet. Syst.*, **31**, 1, 67–86.

Bharath C., Rosales A., Shtessel, Y. and Basin, M. (2017) Chattering analysis of uniform fixed-time convergent Sliding Mode Control. *Journal of the Franklin Institute*, **354**, 4, 1907-1921.

Bhattacharyya, S., Basu, D., Konara, A. and Tibarewala, D. (2015) Interval type-2 fuzzy logic based multiclass ANFIS algorithm for real-time EEG based movement control of a robot arm. *Robotics and Autonomous Systems*, **68**, 9, 104–115.

Buragohain, M. and Mahanta, C. (2008) A novel approach for ANFIS modeling based on full factorial design. *Applied Soft Computing*, **8**, 1, 609–625.

Capisani, L. M., Ferrara A. and Magnani, L. (2007) Second Order Sliding Mode Motion Control of Rigid Robot Manipulators. *Proceedings of the 46th IEEE Conference on Decision and Control New Orleans, LA, USA*, 12-14.

Chang, Y. C. (2000) Robust tracking control for nonlinear MIMO system via fuzzy Approaches. *Automatica*, **36**, 1535-1545.

Cheng, L., Guang Hou Z. and Tan, M. (2009) Adaptive neural network tracking control for manipulators with uncertain kinematics, dynamics and actuator model. *Automatica*, **45**, 10, 2312-2318.

Choi, Y. I. and Cheol Lee, M. (2009) PID Sliding Mode Control for Steering of Lateral Moving Strip in Hot Strip Rolling. *International Journal of Control, Automation, and Systems*, **7**, 3, 399-407.

Elmali, H. and Olgac, N. (1992) Theory and implementation of sliding mode control with perturbation estimation. *IEEE Int. Conf. Robotics Autom.*, **3**, 2114–2119.

Gong, J. Q. and Yao, B. (1999) Adaptive robust control without knowing bounds of parameter variations. *Proc. IEEE Conf. Decision Control*, **4**, 3334–3339.

Ho, H. F., Wong, Y. K. and Rad, A. B. (2007) Robust fuzzy tracking control for robotic manipulators. *Simulat. Model. Pract. Theory*, **15**, 801–816.

Hu, J., Wang, Z., Gao, H. and Stergioulas, L. K. (2012) Robust H_∞ sliding mode control for discrete time-delay systems with stochastic nonlinearities. *Journal of Franklin Institute*, **349**, 1459-1479.

Zheng, E.-H., Xiong, J.-J. and Luo, J.-L. (2014) Second order sliding

mode control for a quadrotor UAV. *ISA Transactions*, **53**.

Jafarov, E. M., Parlakçı, M. N. A. and Istefanopulos, Y. (2005) A new variable structure PID-controller design for robot manipulators. *IEEE Transactions on Control Systems Technology*, **13**, 1, 122-130.

Jang, J. (1993) ANFIS: adaptive-network-based fuzzy inference systems. *IEEE Transactions on Systems, Man and Cybernetics*, **23**, 3, 665–685.

Kar, S., Das, S. and Ghosh, P. K. (2014) Applications of neuro fuzzy systems: A brief review and future outline. *Applied Soft Computing*, **15**, 20, 243–259.

Komsta, J., Oijen, N. and Antoszkiewicz, P. (2013) Integral sliding mode compensator for load pressure control of diecushion cylinder drive. *Control Engineering Practice*. **21**, 708–718.

Li, J., Li, W. and Li, Q. (2012) Sliding mode control for uncertain chaotic systems with input nonlinearity. *Communications in Nonlinear Science and Numerical Simulation*, **17**, 341-348.

Mahmoodabadi, M. J., Taherkhorsandi, M. and Bagheri, A. (2014) Optimal robust sliding mode tracking control of a biped robot based on ingenious multi-objective PSO. *Neurocomputing*, **124**, 194-209.

Melin, P. and Castillo, O. (2005) Intelligent control of a stepping motor drive using an adaptive neuro-fuzzy inference system. *Information Sciences*, **170**, 8, 133-150.

Ortega, R. and Spong, M. (1989) Adaptive motion control of rigid robots: A tutorial. *Automatica*, **25**, 6, 877-888.

Ouyang, P. R., Acob, J. and Pano, V. (2014) PD with sliding mode control for trajectory tracking of robotic system. *Robotics and Computer-Integrated Manufacturing*, **30**, 189–200.

Prasad, S., Purwar, S. and Lishor, N. (2017) Non-linear sliding mode load frequency control in multi-area power system. *Control Engineering Practice*, **61**, 81–92.

Siciliano, B., Sciavicco, L., Villani, L. and Oriolo, G. (2009) *Robotics Modelling, Planning and Control*. Springer-Verlag, London.

Siciliano, B. and Khatib, O. (2008) *Springer Handbook of Robotics*. Springer-Verlag, Berlin Heidelberg.

Su, C. Y., Leung, T. P. (1993) A sliding mode controller with bound estimation for robot manipulators. *IEEE Transactions on Robotics and Automation*, **9**, 2, 208-214.

Sumathi, S. and Surekha, P. (2010) *Computational Intelligence Paradigms Theory and Applications using MATLAB*. CRC Press, Taylor and Francis Group, Boca Raton, LLC.

Sun, T., Pei, H., Pan, Y., Zhou, H. and Zhang, C. (2011) Neural network-based sliding mode adaptive control for robot manipulators. *Neurocomputing*, **74**, 2377-2384.

Utkin, V., Guldner, J. and Shi, J. (2000) *Sliding Mode Control in Electromechanical Systems*. CRC Press LLC.

Wang, J., Zong, Q., Su, R. and Tian, B. (2014) Continuous high order sliding mode controller design for a flexible air-breathing hypersonic vehicle. *ISA Transactions*, **53**, 690–698.

Xiang, W. and Chen, F. (2011) An adaptive sliding mode control scheme for a class of chaotic systems with mismatched perturbations and input nonlinearities. *Communications in Nonlinear Science and Numerical Simulation*, **16**, 1-9.

Yu, H. and Lloyd, S. (1997) Variable structure adaptive control of robot manipulators. *IEEE Proceedings - Control Theory and Applications*, **144**, 167-176.

Zeinali, M. and Notash, L. (2010) Adaptive sliding mode control with uncertainty estimator for robot manipulators. *Mechanism and Machine Theory*, **45**, 1, 80-90.